

Distorted dislocations and OAM spectra of twisted partially coherent noncanonical vortex-pair beams in non-Kolmogorov atmospheric turbulence

Chao Mei(梅超), Ke Cheng(程科), Hao Guo(郭豪), and Xiao-Wen Yi(易小雯)
Citation: Chin. Phys. B, 2026, 35 (**6**): 064207. DOI: 10.1088/1674-1056/ae07c1
http://cpb.iphy.ac.cn; http://iopscience.iop.org/cpb

What follows is a list of articles you may be interested in

Mode and orbital angular momentum controlling of nonlocal solitons by anisotropic diffraction

Junying Zhu(朱俊英), Qing Wang(王清), and Jianning Wei(魏健宁)
Chin. Phys. B, 2026, 35 (**4**): 044202. DOI: 10.1088/1674-1056/ae0163

Precision flatness measurement based on orbital angular momentum

Feifei Han(韩菲菲), Zhiwan Wang(王志琬), Le Wang(王乐), and Shengmei Zhao(赵生妹)
Chin. Phys. B, 2025, 34 (**5**): 054204. DOI: 10.1088/1674-1056/adbd14

Fusion of fractional vortex pairs and their transition to integer vortex controlled by optical power

Chunzhi Sun(孙春志), Xiangwei Chen(陈向炜), Huizhong Xu, and Guo Liang(梁果)
Chin. Phys. B, 2025, 34 (**5**): 054202. DOI: 10.1088/1674-1056/adb8b9

Controlled propagation and particle manipulation of off-axis-rotating elliptical Gaussian beams in strong nonlocal media

Rong-Quan Chen(陈荣泉), Rui-Lin Xiao(肖瑞林), Wei Wang(王伟), Xi-Xi Chu(储茜茜), Yu-Qing Song(宋雨晴), Xu-Dong Hu(胡旭东), and Ming Chen(陈明)
Chin. Phys. B, 2025, 34 (**3**): 034205. DOI: 10.1088/1674-1056/ada9dd

Interface state-based bound states in continuum and below-continuum-resonance modes with high-*Q* factors in the rotational periodic system

Jialing Yang(杨嘉玲), Aoqian Shi(史奥芊), Yuchen Peng(彭宇宸), Peng Peng(彭鹏), and Jianjun Liu(刘建军)
Chin. Phys. B, 2024, 33 (**8**): 084206. DOI: 10.1088/1674-1056/ad4630

Distorted dislocations and OAM spectra of twisted partially coherent noncanonical vortex-pair beams in non-Kolmogorov atmospheric turbulence

Chao Mei(梅超)[1], Ke Cheng(程科)[1,2,†], Hao Guo(郭豪)[1], and Xiao-Wen Yi(易小雯)[1]

[1] *College of Optoelectronic Engineering, Chengdu University of Information Technology, Chengdu* 610225, *China*
[2] *Intelligent Manufacturing Industry Technology Research Institute, Sichuan University of Arts and Science, Dazhou* 635000, *China*

(Received 29 June 2025; revised manuscript received 13 September 2025; accepted manuscript online 17 September 2025)

The twist phase has recently exhibited better resistance to turbulence-induced degeneration of the signal mode in orbital angular momentum (OAM) spectra. However, our attention is paid to exploring the combined influence of the twist factor and noncanonical strength on "distorted dislocation" and OAM spectra in non-Kolmogorov atmospheric turbulence by introducing a noncanonical vortex-pair to twisted partially coherent beams. It is found that the twist factor or noncanonical strength can distort concentric ring dislocations in spatial correlation singularities into the so-called "distorted dislocations". In turbulence propagation, noncanonical strengths can lead to annihilation and creation of distorted dislocations and change the number of dislocations, but twist factors cannot affect their number except for deepening the distortion in the structures. The explicit expression of the OAM flux density per photon, which was also derived, indicates that noncanonical strength can further improve the OAM capacity even if the twist factor reaches its extreme value. Compared to the twist factor, the noncanonical strength plays a more significant role in the signal modulation and detectivity of OAM spectra. If the combined effect of the twist factor and noncanonical strength is considered, the detection performance of the signal mode during long-distance turbulence propagation is distinctly better than that of only the twist factor or the noncanonical strength. The noncanonical strength should not be ignored due to its better performance in the OAM capacity and detection probability of the signal mode. This work may provide inspiration for OAM-based optical communication by the modulation of multi-degrees of freedom associated with noncanonical strengths and twist factors.

Keywords: orbital angular momentum, noncanonical vortex-pair, twist phase, correlation singularity, atmospheric turbulence

PACS: 42.55.–f, 42,68.Ay, 42.50.Tx

DOI: 10.1088/1674-1056/ae07c1 **CSTR:** 32038.14.CPB.ae07c1

1. Introduction

In the past two decades, special phase singularities hidden in the correlation function of partially coherent optical fields have stimulated considerable enthusiasm in theory and application.[1–9] In the spatial frequency domain, these singularities in the correlation function, or cross-spectral density, typically manifest in two different forms: correlation vortex (or coherence vortex) and ring dislocation due to their different topological structures, where their phases are undefined in zero-value of the correlation function.[1,3,10] Sometimes a mixed singularity of the vortex-dislocation also exists. A phase π-jump in the correlation function across ring dislocation boundaries will occur. Ring dislocations of the correlation function with lower spatial coherence can be found, and their numbers equal $N = 2p + |l|$ with radial and azimuthal indices (p, l) in a partially coherent optical field,[11] where the azimuthal index is also the topological charge (TC) of the optical vortex. Recently, a perfect correlation vortex with slow diffraction even in strong atmospheric turbulence over moderate distances has been studied by Ponomarenko *et al.*[12] The coherence vortex generated by binary pinholes has been investigated by Singh *et al.*[13] Fractional coherence vortices resulting from the scattering of fractional vortex beams have also been explored by Vanitha *et al.*[14] Liu and Cai *et al.* generated coherence vortices at specific propagation distances by designing partially coherent light sources with Fourier transform.[15]

On the other hand, optical vortex beams with helical phase can carry orbital angular momentum (OAM) equivalent to $l\hbar$ per photon ($\hbar$ reduced Planck constant).[16] A single photon with more than $10000\hbar$ of OAM states has been generated by Zeilinger *et al.* in 2016,[17] which expands further applications in optical communication, computing, manipulation, and precision metrology.[18–22] The twist phase in partially coherent wavefields has recently attracted great interest due to its essential role in ghost imaging, particle rotation, and reducing turbulence scintillation.[23–27] For example, Zhao *et al.* have studied intensity rotation angles in asymmetric dark hollow structures adjusted by the twist factor, and the resistance to turbulence-induced degeneration of detection mode has also been emphasized by Wang and Cai *et al.*. Additionally, mul-

†Corresponding author. E-mail: ck@cuit.edu.cn

© 2026 Chinese Physical Society and IOP Publishing Ltd. All rights, including for text and data mining, AI training, and similar technologies, are reserved.

tiple vortices in optical fields can produce topological dynamics and interactions among vortices, such as vortex collisions, creation, and annihilation. Off-axis double-vortex beams with multiple different vortices possessing more control potentials in OAM have been introduced in fully and partially coherent fields by Gu *et al.* and Liu *et al.*, respectively.[28,29] By combining twisted phases and double-vortex structures, their propagation in atmospheric turbulence has been further explored by Qu *et al.*[30] Specifically, vortex-pair beams carrying a pair of vortices can be divided into two categories: one is a vortex dipole with opposite vortices, and the other is an isopolar vortex pair with identical vortices. In 2025, Wang *et al.* explored the dynamic evolution of vortex-pair beams and observed their helical and intertwined behaviors, like a vortex-pair dance and oscillation.[31] However, these studies are based entirely on canonical double-vortex or vortex-pair structures. The natural question to ask is what happens to their spatial correlation singularities and OAM in turbulence propagation if a noncanonical vortex pair is embedded.

The purpose of this paper is to explore the competitive and cooperative influences of the twist phase and the noncanonical vortex of twisted partially coherent noncanonical vortex-pair beams (TPCNVPBs) on spatial correlation singularities and OAM in turbulence propagation, where novel dislocation structures in correlation singularities are found and the embedded noncanonical vortex-pair demonstrates a more remarkable ability to improve OAM capacity and signal detectivity of OAM mode compared to the twist factor. This work may be useful for OAM-based optical communication, imaging, sensing, and optical computing using additional freedom with a noncanonical vortex.

2. Distorted dislocations in twist phase and noncanonical vortex-pair

In the polar coordinate system, the electric field of the Gaussian beam carrying a noncanonical vortex pair at the source plane ($z=0$) can be expressed as[1]

$$E(\boldsymbol{r},0)=F(\boldsymbol{r})G(\boldsymbol{r})\exp(\mathrm{i}\zeta). \tag{1}$$

Here, $\boldsymbol{r}=(x,y)$ is the position vector in the source plane, ζ is an arbitrary phase, $G(\boldsymbol{r})$ is a Gaussian-profile beam with a waist width of w, and $F(\boldsymbol{r})$ is the function of the noncanonical vortex pair described by[32]

$$\begin{aligned}F(\boldsymbol{r})=F(x,y)\ =\ &[(x-d)+\mathrm{i}\,\mathrm{sgn}(l_1)Qy]^{|l_1|}\\ &\times[(x+d)+\mathrm{i}\,\mathrm{sgn}(l_2)Qy]^{|l_2|},\end{aligned} \tag{2}$$

where l_1 and l_2 are the topological charges of the off-axis optical vortices, d is the off-axis distance of the noncanonical vortex pair in the x-direction, and sgn is the sign function. The complex parameter Q in Eq. (2) denotes the noncanonical strength of the optical vortex, and $Q=\pm1$ denotes the canonical or symmetric vortex. Although the phase is distorted by the complex parameter Q, the conservation of TC in a noncanonical vortex is still valid. If the statistical distribution of any phase ζ corresponds to the correlation of the Schell model[33]

$$C(|\boldsymbol{r}_1-\boldsymbol{r}_2|)=\exp\left(-|\boldsymbol{r}_1-\boldsymbol{r}_2|^2/\sigma^2\right), \tag{3}$$

where σ is the transverse coherence length.

For a quasi-monochromatic optical field, the twisted partially coherent noncanonical vortex-pair beams (TPCNVPBs) are structured by embedding a noncanonical vortex pair into twisted partially coherent beams, and their cross-spectral density at $z=0$ is expressed as[23]

$$W(\boldsymbol{r}_1,\boldsymbol{r}_2,0)=\langle E^*(\boldsymbol{r}_1,0)E(\boldsymbol{r}_2,0)\rangle\exp[-\mathrm{i}k\mu_0\boldsymbol{r}_1\times\boldsymbol{r}_2], \tag{4}$$

where $\langle\ \rangle$ denotes the ensemble averaging, $k=2\pi/\lambda$ is the wavenumber with λ being the beam wavelength. μ_0 is the twist factor of the twist phase. The positive or negative value of μ_0 determines the clockwise or counterclockwise rotation direction along the optical axis during propagation, respectively. Its value is limited by the inequation[34]

$$|\mu_0|\le\left(k\sigma^2\right)^{-1}. \tag{5}$$

The twist phase only exists in partially coherent beams because its value is zero for the coherence length σ approaching positive infinity. Additionally, a larger absolute value of μ_0 means a more severe twist phase.

The cross-spectral density of the TPCNVPBs propagating in atmospheric turbulence along the z-axis follows the generalized Huygens–Fresnel integral with the expression[33]

$$\begin{aligned}&W(\boldsymbol{\rho}_1,\boldsymbol{\rho}_2,z)\\ &=\left(\frac{k}{2\pi z}\right)^2\iint_\infty W(\boldsymbol{r}_1,\boldsymbol{r}_2,0)\\ &\quad\times\exp\left[-\frac{\mathrm{i}k}{2z}(\boldsymbol{r}_1-\boldsymbol{\rho}_1)^2+\frac{\mathrm{i}k}{2z}(\boldsymbol{r}_2-\boldsymbol{\rho}_2)^2\right]\\ &\quad\times\langle\exp[\psi^*(\boldsymbol{r}_1,\boldsymbol{\rho}_1,z)+\psi(\boldsymbol{r}_2,\boldsymbol{\rho}_2,z)]\rangle\,\mathrm{d}\boldsymbol{r}_1\,\mathrm{d}\boldsymbol{r}_2.\end{aligned} \tag{6}$$

Here $\boldsymbol{\rho}_1$ and $\boldsymbol{\rho}_2$ are position vectors of two points in the receiver plane, and $\psi(\boldsymbol{r},\boldsymbol{\rho},z)$ is a phase perturbation in atmospheric turbulence. Its Rytov approximation is expressed as[35]

$$\begin{aligned}&\langle\exp[\psi^*(\boldsymbol{r}_1,\boldsymbol{\rho}_1,z)+\psi(\boldsymbol{r}_2,\boldsymbol{\rho}_2,z)]\rangle\\ &=\exp\left[-\frac{(\boldsymbol{r}_1-\boldsymbol{r}_2)^2+(\boldsymbol{r}_1-\boldsymbol{r}_2)(\boldsymbol{\rho}_1-\boldsymbol{\rho}_2)+(\boldsymbol{\rho}_1-\boldsymbol{\rho}_2)^2}{\rho_0^2}\right],\end{aligned} \tag{7}$$

with $1/\rho_0^2=\pi^2k^2z\int_0^\infty\kappa^3\Phi(\kappa,\alpha)\,\mathrm{d}\kappa/3$, where $\Phi(\kappa,\alpha)$ is the non-Kolmogorov power spectrum, which can be expressed by the following formula:

$$\Phi(\kappa,\alpha)=A(\alpha)C_n^2\frac{\exp\left(-\kappa^2/\kappa_m^2\right)}{\left(\kappa^2+\kappa_0^2\right)^{\alpha/2}}, \tag{8}$$

where C_n^2 is the turbulence structure constant, κ is the spatial frequency magnitude, and α is a generalized exponential factor for $3<\alpha<4$. The non-Kolmogorov spectrum can be reduced to the standard Kolmogorov spectrum when $\alpha=11/3$, $L\to\infty$, and $l\to=0$. When the beams propagate through non-Kolmogorov atmospheric turbulence along a vertical path,[36] one can obtain the expression

$$\begin{aligned}\frac{1}{\rho_0^2} &= \frac{k^2 z C_n^2 \cos(\alpha\pi/2)}{24(\alpha-2)}\Gamma(\alpha-1)\\ &\times\left[\left(2\kappa_0^2-2\kappa_m^2+\alpha\kappa_m^2\right)\kappa_m^{2-\alpha}\right.\\ &\left.\times\exp\left(\frac{\kappa_0^2}{\kappa_m^2}\right)\Gamma\left(2-\frac{\alpha}{2},\frac{\kappa_0^2}{\kappa_m^2}\right)-2\kappa_0^{4-\alpha}\right],\end{aligned}\tag{9}$$

where Γ denotes the Gamma function. The parameters $\kappa=2\pi/L_0$ and $\kappa_m=c(\alpha)/l_0$ in Eq. (8) are related by the outer and inner scales L_0 and l_0 of atmospheric turbulence with

$$c(\alpha)=\left[\frac{\Gamma(\alpha-1)}{6\pi}\Gamma\left(\frac{5-\alpha}{2}\right)\cos\left(\frac{\alpha\pi}{2}\right)\right]^{1/(\alpha-5)}.\tag{10}$$

Substituting Eqs. (4), (7)–(10) into Eq. (6) and using the following formula:

$$(x+\mathrm{i}y)^l=\sum_{s=0}^{l}\frac{l!}{s!(l-s)!}x^{l-s}(\mathrm{i}y)^s,\tag{11}$$

$$\begin{aligned}&\int_{-\infty}^{+\infty}x^n\exp\left(-px^2+2qx\right)\mathrm{d}x\\ &=n!\exp\left(\frac{q^2}{p}\right)\left(\frac{q}{p}\right)^n\sqrt{\frac{\pi}{p}}\sum_{k=0}^{[n/2]}\frac{1}{k!(n-2k)!}\left(\frac{p}{4q^2}\right)^k,\end{aligned}\tag{12}$$

the cross-spectral density of the TPCNVPBs with topological charges of l_1 and l_2 at the receiver plane in non-Kolmogorov turbulence can be obtained as

$$\begin{aligned}W(\boldsymbol{\rho}_1,\boldsymbol{\rho}_2,z) &= \left(\frac{k}{2\pi z}\right)^2\exp\left[\frac{\mathrm{i}k}{2z}\left(\boldsymbol{\rho}_1^2-\boldsymbol{\rho}_2^2\right)\right]\exp\left[-\frac{(\boldsymbol{\rho}_1-\boldsymbol{\rho}_2)^2}{\rho_0^2}\right]\\ &\times\sum_{s_1=0}^{l_1}\sum_{s_2=0}^{l_2}\sum_{s_3=0}^{l_1}\sum_{s_4=0}^{l_2}\sum_{q_1}^{s_1+s_2}\sum_{q_2}^{s_3+s_4}\frac{l_1!d^{l_1-s_1}}{s_1!(l_1-s_1)!}\frac{l_2!(-d)^{l_2-s_2}}{s_2!(l_2-s_2)!}\frac{l_1!d^{l_1-s_3}}{s_3!(l_1-s_3)!}\frac{l_2!(-d)^{l_2-s_4}}{s_4!(l_2-s_4)!}\frac{(s_1+s_2)!(-\mathrm{i}Q^*)^{q_1}}{q_1!(s_1+s_2-q_1)!}\\ &\times\frac{(s_3+s_4)!(\mathrm{i}Q)^{q_2}}{q_2!(s_3+s_4-q_2)!}c_1!\sqrt{\frac{\pi}{p_1}}\left(\frac{1}{p_1}\right)^{c_1}\exp\left(\frac{a_1^2}{p_1}\right)\sum_{e_1=0}^{[c_1/2]}\frac{1}{(c_1-2e_1)!e_1!}\left(\frac{p_1}{4}\right)^{e_1}\\ &\times\sum_{v_1=0}^{c_1-2e_1}\frac{(c_1-2e_1)!}{v_1!(c_1-2e_1-v_1)!}a_1^{c_1-2e_1-v_1}\sum_{v_2=0}^{v_1}\frac{v_1!}{v_2!(v_1-v_2)!}\left(\frac{1}{\sigma^2}+\frac{1}{\rho_0^2}\right)^{v_1-v_2}\left(-\frac{\mathrm{i}k\mu_0}{2}\right)^{v_2}c_2!\sqrt{\frac{\pi}{p_2}}\left(\frac{1}{p_2}\right)^{c_2}\\ &\times\exp\left(\frac{a_2^2}{p_2}\right)\sum_{e_2=0}^{[c_2/2]}\frac{1}{(c_2-2e_2)!e_2!}\left(\frac{p_2}{4}\right)^{e_2}\sum_{v_3=0}^{c_2-2e_2}\frac{(c_2-2e_2)!}{v_3!(c_2-2e_2-v_3)!}a_2^{c_2-2e_2-v_3}\sum_{v_4=0}^{v_3}\frac{v_3!}{v_4!(v_3-v_4)!}\\ &\times\left(\frac{\mathrm{i}k\mu_0}{2}\right)^{v_3-v_4}\left(-\frac{\left(1/\sigma^2+1/\rho_0^2\right)\mathrm{i}k\mu_0}{2p_1}\right)^{v_4}c_3!\sqrt{\frac{\pi}{p_3}}\left(\frac{1}{p_3}\right)^{c_3}\exp\left(\frac{a_3^2}{p_3}\right)\sum_{e_3=0}^{[c_3/2]}\frac{1}{(c_3-2e_3)!e_3!}\left(\frac{p_3}{4}\right)^{e_3}\\ &\times\sum_{v_5=0}^{c_3-2e_3}\frac{(c_3-2e_3)!c_4!a_3^{c_3-2e_3-v_5}b_1^{v_5}}{v_5!(c_3-2e_3-v_5)!}\sqrt{\frac{\pi}{p_4}}\left(\frac{1}{p_4}\right)^{c_4}\exp\left(\frac{a_4^2}{p_4}\right)\sum_{e_4=0}^{[c_4/2]}\frac{1}{(c_4-2e_4)!e_4!}\left(\frac{p_4}{4a_4^2}\right)^{e_4}\end{aligned}\tag{13}$$

with

$$\begin{aligned}&p_1=\frac{1}{w_0^2}+\frac{\mathrm{i}k}{2z}+f,\quad p_2=\frac{1}{w_0^2}-\frac{\mathrm{i}k}{2z}-\frac{f^2}{p_1}-f,\\ &p_3=p_1+\frac{k^2\mu_0^2}{4p_2},\\ &p_4=p_2+\frac{k^2\mu_0^2}{4p_1}+\frac{f^2k^2\mu_0^2}{4p_1^2p_2}-\frac{b_1^2}{p_3},\end{aligned}\tag{14}$$

$$a_1=\frac{\mathrm{i}k\rho_{1x}}{2z}-\frac{\rho_{1x}-\rho_{2x}}{2\rho_0^2},\tag{15}$$

$$\begin{aligned}a_2&=\frac{fa_1}{p_1}-\frac{\mathrm{i}k\rho_{2x}}{2z}+\frac{\rho_{1x}-\rho_{2x}}{2\rho_0^2},\\ a_3&=\frac{\mathrm{i}k\mu_0a_2}{2p_2}+\frac{\mathrm{i}k\rho_{1y}}{2z}-\frac{\rho_{1y}-\rho_{2y}}{2\rho_0^2},\end{aligned}\tag{16}$$

$$\begin{aligned}a_4&=-\frac{\mathrm{i}k\rho_{2y}}{2z}+\frac{\rho_{1y}-\rho_{2y}}{2\rho_0^2}-\frac{\mathrm{i}k\mu_0a_1}{2p_1}-\frac{\mathrm{i}k\mu_0a_2f}{2p_1p_2}+\frac{a_3b_1}{p_3},\\ b_1&=f+\frac{fk^2\mu_0^2}{4p_1p_2},\end{aligned}\tag{17}$$

$$f=1/\sigma^2+1/\rho_0^2,\quad c_1=s_1+s_2-q_1,$$

$$c_2=s_3+s_4-q_2+v_1-v_2,\tag{18}$$

$$c_3=q_1+v_3-v_4,\quad c_4=q_2+v_2+v_4+v_5.\tag{19}$$

The spatial correlation singularities at the receiver plane can be derived by $\chi(\boldsymbol{\rho})=W(\boldsymbol{\rho},-\boldsymbol{\rho},z)=0$, which generally presents concentric ring dislocations,[11] and their phases experience π-jump across these concentric ring dislocation boundaries. The number of concentric ring dislocations equals the absolute value of the topological charge of the optical vortex,

i.e., $N = |l_1| + |l_2|$, if the embedded on-axis optical vortex is canonical.[37] However for the twisted partially coherent beams carrying noncanonical vortexpair, what will happen for spatial correlation singularities in non-Kolmogorov atmospheric turbulence?

Large amounts of numerical calculations using the derived Eqs. (13)–(19) are carried out to illustrate the dependence of spatial correlation singularities on noncanonical strength, twist factor, and propagation distance in non-Kolmogorov atmospheric turbulence. Typical examples are compiled in Figs. 1–3. The calculation parameters are $\lambda = 632.8$ nm, $l_1 = l_2 = +2$, $L_0 = 1$ m, $l_0 = 1$ cm, $\alpha = 3.67$, $C_n^2 = 10^{-14}$ m$^{-2/3}$, $w_0 = 1$ mm, $\sigma = w_0$, $d = 0.5w_0$, and Rayleigh length $z_0 = kw_0^2/2$ unless otherwise stated.

Figure 1 shows spatial correlation singularities of TPCNVPBs with canonical vortex-pair of $l_1 = l_2 = +2$ for different twist factors at $z = 2z_0$ in non-Kolmogorov atmospheric turbulence, where the case of on-axis $d = 0$ is also plotted for comparison. In the case of canonical vortex-pair, spatial correlation singularities exhibit concentric ring dislocations with zero-value in cross-spectral density for $d = 0$ in Fig. 1(a), and for $d \neq 0$ those ring dislocations change into irregular or tilted ones due to their intensity disproportion in radial directions resulting from the twist factor μ_0. The circular symmetry of the ring dislocations is broken by an increase of the off-axis distance. Evidently, the number of ring or irregular dislocations is equal to the total topological charge $N = |l_1| + |l_2| = 4$ for canonical vortex-pair as illustrated in Fig. 1. It needs to be emphasized that their dislocation numbers cannot be altered by the twist factor alone. A larger off-axis distance tends to separate the dislocations into non-concentric ones with a negative twist factor of $\mu_0 < 0$, but for a positive twist factor of $\mu_0 > 0$ those concentric structures remain in Figs. 1(b) and 1(c). The phenomena indicate that the twist factor in the existence of off-axis vortices can lead to the circular symmetry breaking of traditional ring dislocations, which also results in the so-called "distorted dislocations" in spatial correlation singularities. It should be noted that the proposed TPCNVPBs intrinsically possess twisted structures in dislocated dislocation. Even when they propagate in free space, these dislocations also change from $N = 4$ to $N = 2$, which indicates that the dislocated dislocations intrinsically exist in the beams, and are not unique to turbulence. More details in free-space propagation are available in Fig. A1 of Appendix A, where one can find the dark core is divided into four dislocations from $z = 0$ to $z = 0.8z_0$, and they gradually reduce into two dislocations at $z = 1.2z_0$ even when the proposed beams propagate in free space.

Figure 2 further illustrates distorted dislocations of TPCNVPBs with a noncanonical vortex-pair with different noncanonical strengths and twist factors at $z = 10z_0$ in non-Kolmogorov atmospheric turbulence, which are marked by white dashed lines. One can find that the number and structure of distorted dislocations are sensitive to the noncanonical strength because the distorted dislocations are $N = 2$ rather than $N = 4$ within the range of $1 + 0.12\mathrm{i} \leq Q \leq 1 + 0.23\mathrm{i}$ for $\mu_0 = 0$ as shown in Figs. 2(a1)–2(a4), which indicates that only noncanonical strength can change dislocation numbers. The twist factor alone is not sufficient to change the number of dislocations. Similar cases can also be found in the condition of $1 + 0.03\mathrm{i} \leq Q \leq 1 + 0.14\mathrm{i}$ for $\mu_0 = -0.1$ m^{-1} and $1 + 0.28\mathrm{i} \leq Q \leq 1 + 0.33\mathrm{i}$ for $\mu_0 = 0.1$ m^{-1} in Figs. 2(b1)–2(c4). The topological structure (see red dashed circles) in distorted dislocations can be adjusted by slight changes in noncanonical strength as shown in Figs. 2(c1)–2(c4), where their dislocations annihilate from $N = 4$ in $Q = 1 + 0.27\mathrm{i}$ to $N = 2$ in $Q = 1 + 0.28\mathrm{i}$, and then generate from $N = 2$ in $Q = 1 + 0.33\mathrm{i}$ to $N = 4$ in $Q = 1 + 0.34\mathrm{i}$. The topological evolution with annihilation and creation of distorted dislocations in partially coherent beams is similar to that of the vortex core in a fully coherent optical field. The results indicate that the number of distorted dislocations in the presence of noncanonical strength Q does not always satisfy the conventional equation of $N = |l_1| + |l_2|$, or that noncanonical strength can lead to the number of distorted dislocations $N \neq |l_1| + |l_2|$. Twist factors can further deepen dislocation distortion, but do not affect the number of dislocations.

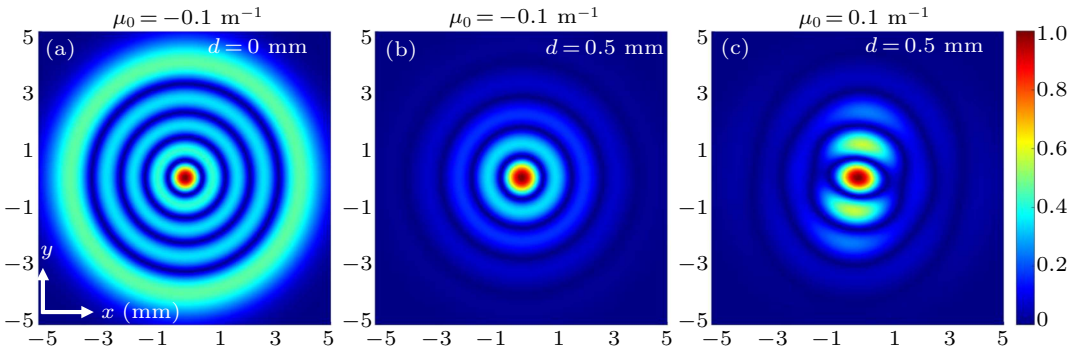


Fig. 1. Distorted dislocations in spatial correlation singularities of TPCNVPBs with canonical vortex-pair ($Q = 1$) of $l_1 = l_2 = +2$ for different twist factors at $z = 2z_0$ in non-Kolmogorov atmospheric turbulence.

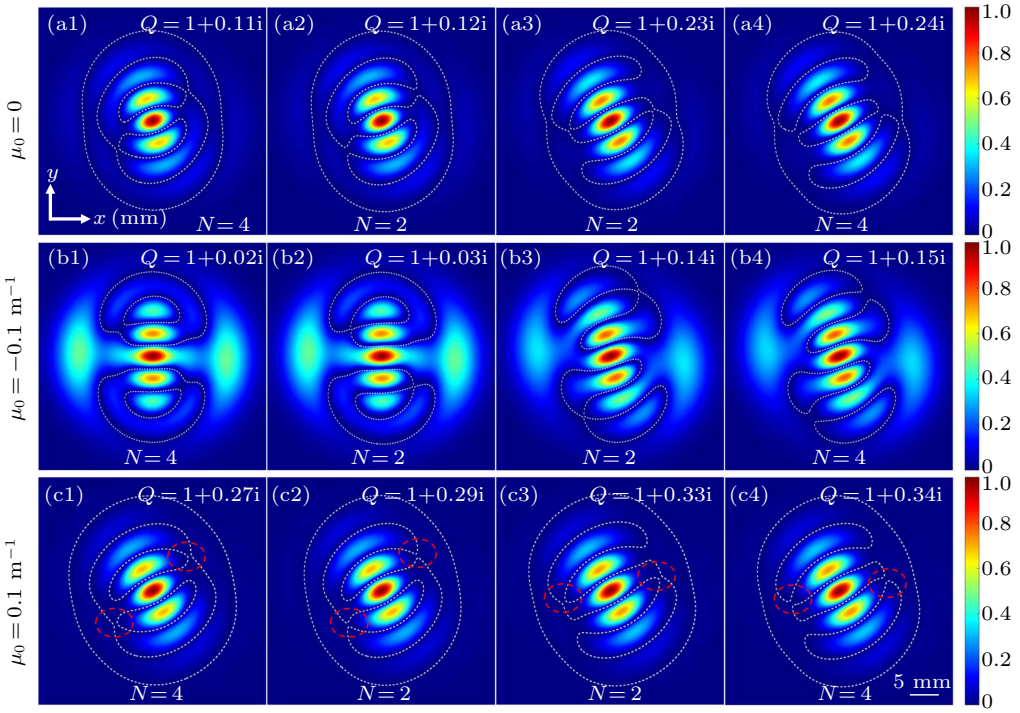


Fig. 2. Distorted dislocations of TPCNVPBs with noncanonical vortex-pair for different noncanonical strengths and twist factors at $z = 10z_0$ in non-Kolmogorov atmospheric turbulence.

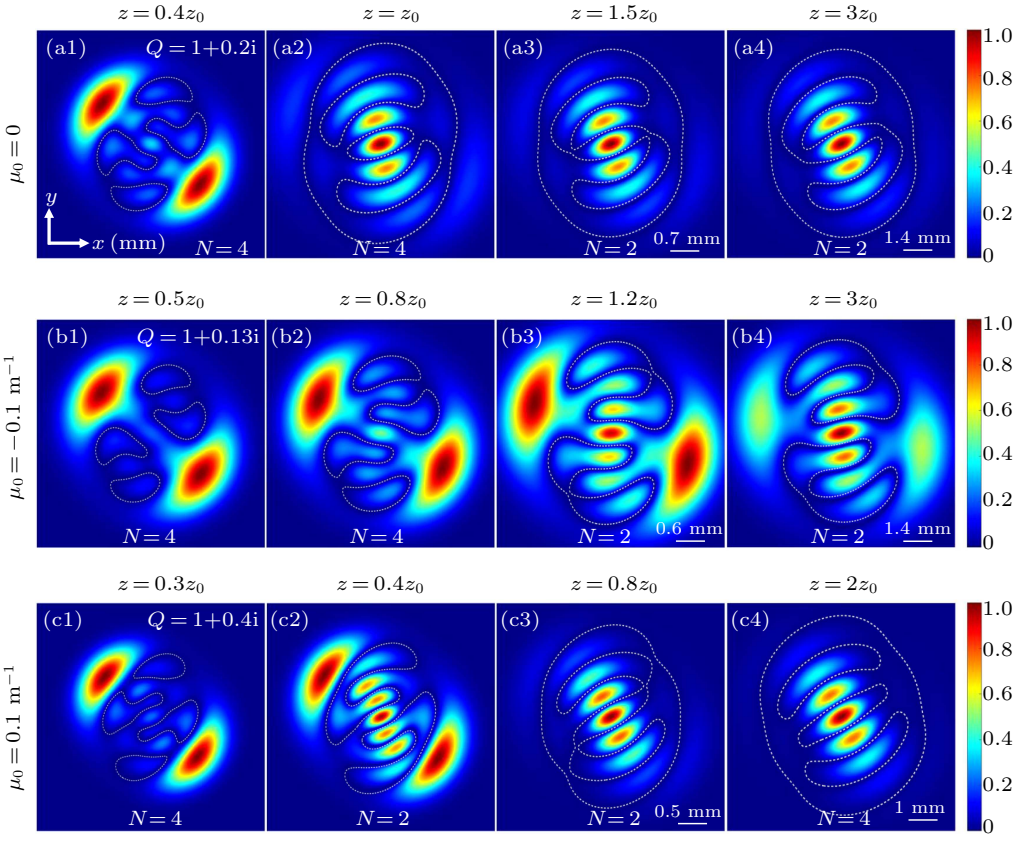


Fig. 3. Dynamics evolution of distorted dislocations of TPCNVPBs with noncanonical vortex-pair for different noncanonical strengths and twist factors in non-Kolmogorov atmospheric turbulence. (a1)–(a4): $Q = 1 + 0.2$i; (b1)–(b4): $Q = 1 + 0.13$i; (c1)–(c4): $Q = 1 + 0.4$i.

Figure 3 further explores the dynamic evolution of distorted dislocations for different twist factors and noncanonical strengths in non-Kolmogorov atmospheric turbulence.

In the absence of twist factors, the number of distorted dislocations can also change in turbulence propagation even with only noncanonical strength in Figs. 3(a1)–3(a4), where their numbers are $N = 4$ for $0 < z \leq z_0$ and $N = 2$ for $z \geq 1.5z_0$, respectively. However, for free-space propagation, their dislo-

cation numbers always remain unchanged with $N=4$. When a twist factor exists, their dislocation structures are further distorted, and the change in dislocation numbers can be found in the dynamics evolution. For example, the distorted dislocations are always $N=2$ for $z \geq 1.2z_0$ in $\mu_0 = -0.1$ m^{-1} in Figs. 3(b3)–3(b4), and $N=2$ for $0.4z \leq z \leq 0.8z_0$ in $\mu_0 = 0.1$ m^{-1} in Figs. 3(c2)–3(c3). More details of the three-dimensional (3D) evolution in Figs. 3(b2)–3(b3) are provided in Fig. A2 of Appendix A, where one can find that topological creation and annihilation in concentric dislocations are impossible because these rings expand with the same amplitude. For the distorted dislocations, the intrinsic distortion in the optical structure leads to topological evolution during propagation. These singular behaviors in dislocation numbers indicate that the embedded noncanonical strength can significantly change the number of dislocations in spatial correlation singularities, but the twist factor is insufficient to alter the number of dislocations, except for its contributions to reinforcing distorted structures. If we encode information into their dislocation structures, perhaps we can find an alternative method to assess turbulence intensity through the dynamical evolution of the number and structure of dislocations in turbulence propagation.

3. OAM spectra in twist phase and noncanonical vortex-pair

For partially coherent beams, the electric field realization $E(\rho, \varphi, z)$ can be decomposed into a superposition of OAM eigenfunctions as

$$E(\rho,\varphi,z) = \frac{1}{\sqrt{2\pi}} \sum_{p=0}^{\infty} \sum_{m=-\infty}^{\infty} a_m(\rho,z) R_p(\rho,z) \exp(\mathrm{i}m\varphi), \quad (20)$$

where m is an integer number, $a_m(\rho,z)$ are complex coefficients, and $R_p(\rho,z)$ comprises a radial basis set. The functions $a_m(\rho,z)$ are given by the integral

$$a_m(\rho,z) = \frac{1}{\sqrt{2\pi}} \sum_{p=0}^{\infty} R_p(\rho,z) \int_0^{2\pi} E(\rho,\varphi,z) \times \exp(-\mathrm{i}m\varphi)\,\mathrm{d}\varphi. \quad (21)$$

The average energy of the OAM mode m contained in a partially coherent beam can be obtained by integrating over the radial direction at

$$P_m = \sum_{p=0}^{\infty} \left\langle |a_m(\rho,\varphi)|^2 \right\rangle = \frac{1}{2\pi} \int_0^{\infty}\int_0^{\infty}\int_0^{2\pi}\int_0^{2\pi} \langle E^*(\rho_1,\varphi_1,z) E(\rho_2,\varphi_2,z)\rangle \mathrm{e}^{\mathrm{i}m(\varphi_1-\varphi_2)} \times \sum_{p=0}^{\infty} R_p^*(\rho_1,z) R_p(\rho_2,z)\, \rho_1\rho_2\,\mathrm{d}\rho_1\,\mathrm{d}\rho_2\,\mathrm{d}\varphi_1\,\mathrm{d}\varphi_2. \quad (22)$$

By applying the radial basis $\sum_{p=0}^{\infty} R_p^*(\rho_1,z) R_p(\rho_2,z) = \delta(\rho_2-\rho_2)/\rho_2$ and integrating over ρ_1, Eq. (22) reduces to[26]

$$P_m = \frac{1}{2\pi} \iiint W(\rho,\varphi_1,\rho,\varphi_2,z)\, \mathrm{e}^{\mathrm{i}m(\varphi_1-\varphi_2)} \rho\,\mathrm{d}\rho\,\mathrm{d}\varphi_1\,\mathrm{d}\varphi_2 \quad (23)$$

with $\rho = \rho_1 = \rho_2$, where $(\rho_1,\varphi_2) = \rho_1$ and $(\rho_2,\varphi_2) = \rho_2$ are the radial and azimuthal coordinates of two points in Eq. (6). The power weight or relative power of $R_m = P_m/\sum P_m$ for the OAM spectra with m-mode can be calculated by Eq. (23). The value of $R_{m=l=l_1+l_2}$ at the z plane can be regarded as the detection probability of the signal mode for the source plane, which shows the propagation efficiency of the signal mode in the spiral spectrum. Its value will decrease due to the power at the signal l-mode spreading to other adjacent modes. Inevitably the crosstalk probability of other modes $R_{m\neq l}$ will increase in turbulence propagation. For simplicity, the central (or signal) and crosstalk (or other adjacent) OAM modes are represented by $\Delta l = m-l = 0$ and $\Delta l = m-l \neq 0$, respectively. The symmetry of OAM spectra can be simply described by $\sum_{m=-\infty}^{\infty} \Delta l = 0$. In general, the relation of $\sum_{m=-\infty}^{\infty} m R_m = \sum_i l_i$ without twist factor and noncanonical strength for free-space propagation is always satisfied.[26]

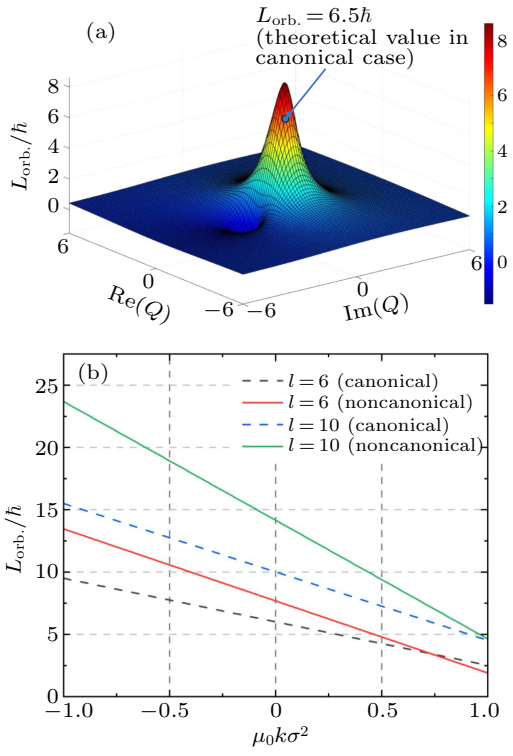


Fig. 4. (a) The effect of noncanonical strength on OAM per photon ($L_{\mathrm{orb.}}$) for $d=0$, $l=4$, and $\mu_0 k\sigma^2 = -1$ at $z=0$. (b) Variation of $L_{\mathrm{orb.}}$ *versus* $\mu_0 k\sigma^2$ for canonical and noncanonical cases for $d=0$ at $z=0$.

On the other hand, the average OAM flux density per photon can also be given by [25,38,39]

$$L_{\mathrm{orb.}}(\boldsymbol{\rho},z) = \hbar \frac{\int \mathrm{Im}\left[\partial_{\varphi_2} W(\boldsymbol{\rho}_1,\boldsymbol{\rho}_2,z)\right]_{\boldsymbol{\rho}_1=\boldsymbol{\rho}_2=\boldsymbol{\rho}} \mathrm{d}^2\boldsymbol{\rho}}{\int W(\boldsymbol{\rho},\boldsymbol{\rho},z)\,\mathrm{d}^2\boldsymbol{\rho}}. \quad (24)$$

For the off-axis distance $d = 0$, we derive the analytical expression of OAM flux density per photon of TPCNVPBs with TC $= l$ at $z = 0$ as

$$L_{\text{orb.}} = \hbar\left(\frac{2l\,\text{Re}\,(Q)}{1+|Q|^2} - \frac{3+|Q|^2}{4\left(1+|Q|^2\right)}\mu_0 k w_0^2 - \frac{|l|\left(3+|Q|^2\right)}{4\left(1+|Q|^2\right)}\mu_0 k w_0^2\right). \tag{25}$$

For the canonical vortex of $Q = 1$, the reduced expression of Eq. (25) is equivalent to Eq. (22) in Ref. [23], and also identical with Eq. (12) in Ref. [25], if the beam width is the same as those in Refs. [23,25]. Different from the OAM per photon equivalent to $l\hbar$, it is found from Eq. (25) that the $L_{\text{orb.}}$ is separated into three parts. The first term is induced by topological charge and noncanonical strength, which can be fractional and less than topological charge l for noncanonical cases. The second term is affected by twist factor and noncanonical strength, and the value of Q can distinctly magnify the influence of twist factor on the $L_{\text{orb.}}$. The third term emphasizes the combined impact of topological charge, twist factor, and noncanonical strength on the $L_{\text{orb.}}$. The effect of noncanonical strength on the $L_{\text{orb.}}$ is illustrated in Fig. 4(a), where the negative twist factor is set to its limit of $\mu_0 k\sigma^2 = -1$ in Eq. (5). One can see that the value of $L_{\text{orb.}}$ is manipulated by the real and imaginary parts of Q from $-\hbar$ to $8\hbar$, and its maximal value exceeds the theoretical value of $6.5\hbar$ in the canonical case. If the real and imaginary parts of $Q = a + \mathrm{i}b$ satisfy

$$\frac{11}{21} < a < 1,$$
$$-\sqrt{\left(a-\frac{11}{21}\right)(1-a)} < b < \sqrt{\left(a-\frac{11}{21}\right)(1-a)}, \tag{26}$$

the OAM capacity in the noncanonical regime exceeds that in the canonical case even when the twist factor μ_0 reaches its extreme value of $\mu_0 k\sigma^2 = -1$. Figure 4(b) plots the variation of $L_{\text{orb.}}$ with the normalized twist factor $\mu_0 k\sigma^2$ for canonical and noncanonical cases. For the extreme value of $\mu_0 k\sigma^2$, $= -1$, the maximum OAM produced by noncanonical strength are $13\hbar$ and $24\hbar$ for $l = 6$ and $l = 10$, but those values are $9\hbar$ and $16\hbar$ in the canonical case, respectively. The results indicate that the noncanonical strength Q can further improve the OAM carried by per photon compared to the canonical case, even if the twist factor is impossible to continue to enhance the OAM capacity.

3.1. Asymmetrical OAM spectra in the source plane

Figures 5 and 6 present the asymmetrical OAM spectra as a function of Δl for different twist factors and noncanonical strengths at $z = 0$, respectively. For canonical vortex pairs in Fig. 5, it can be noticed that the OAM spectra are asymmetric about $\Delta l = 0$ for $\mu_0 \neq 0$, but for $\mu_0 = 0$ their symmetry still exists, which indicates that the twist factors without noncanonical strengths can break the symmetric distribution of the OAM spectra, and the equation $\sum_{m=-\infty}^{\infty} mR_m \neq \sum_i l_i$ is found due to the embedded twist factors at $z = 0$. It should be emphasized that the total OAM of an arbitrary paraxial beam of $J = \sum_{m=-\infty}^{\infty} mP_m$ is always valid regardless of whether the OAM spectra are symmetric or not. Only because the ratio of J to $P = \sum P_m$ is not equal to TC (see Eq. (25)) in asymmetric OAM spectra, which results in the conclusion of $\sum_{m=-\infty}^{\infty} mR_m \neq \sum_i l_i$. Moreover, the negative twist factor $\mu_0 < 0$ gives the spiral spectra with $\Delta l > 0$ clear advantages, whereas for $\mu_0 > 0$ the case is opposite. It can be explained that the OAM capacity can be improved by negative μ_0 based on Eq. (25). The more modes in the range of $\Delta l > 0$ there are, the better it is to ensure the increase in OAM capacity. For example, the maximal weights of $\mu_0 = 0.05\ \text{m}^{-1}$ and $0.1\ \text{m}^{-1}$ in Figs. 5(d)–5(e) are concentrated at $\Delta l = -1$ and -2 rather than $\Delta l = 0$ for $\mu_0 = 0$. Similar cases can also be found for $\mu_0 = -0.1\ \text{m}^{-1}$ and $-0.05\ \text{m}^{-1}$ in Figs. 5(a) and 5(b).

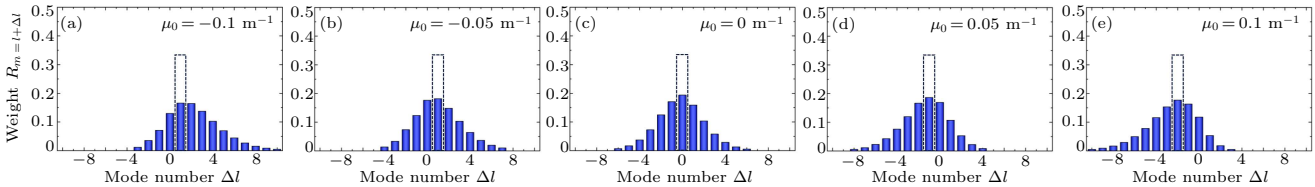


Fig. 5. Asymmetrical OAM spectra of TPCNVPBs with canonical vortex-pair ($Q = 1$) for different twist factors at $z = 0$: (a)–(b), $\mu_0 < 0$; (c) $\mu_0 = 0$; (d)–(e) $\mu_0 > 0$.

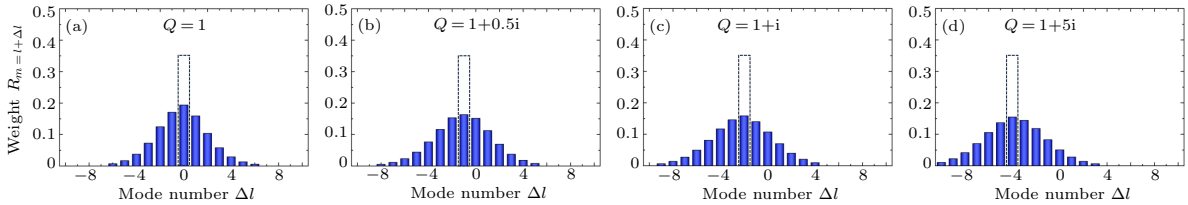


Fig. 6. Asymmetrical OAM spectra of TPCNVPBs with noncanonical vortex pairs without twist factor ($\mu_0 = 0$) at $z = 0$. Note that (a) the canonical case of $Q = 1$ is presented for comparisons.

For noncanonical strengths without twist factors in Figs. 6(b)–6(d), one can find that the OAM modes for $\Delta l < 0$ gradually dominate as the noncanonical strength deviates from $Q = 1 + 0.5\mathrm{i}$, $Q = 1 + \mathrm{i}$ to $Q = 1 + 5\mathrm{i}$, where their maximal modes are located at $\Delta l = -1$, -2, and -4, respectively. A similar case for the dominated $\Delta l < 0$ will also occur if one increases the real part of the noncanonical strength. Twist factors or noncanonical strengths can lead to asymmetrical phase distributions. The asymmetric spiral spectra can be attributed to the fact that twist factors or noncanonical strengths can lead to asymmetrical phase distributions and significantly change the power or energy weight of spiral modes in a disproportionate form.

3.2. Asymmetrical OAM spectra in non-Kolmogorov atmospheric turbulence

From Figs. 5 and 6, one can clearly find that negative twist factors promote the dominance of $\Delta l > 0$, but the spiral spectra are dominated by $\Delta l < 0$ at a larger noncanonical strength. This raises an interesting question for negative twist factors and noncanonical strengths. Figure 7 further gives the combined effect of negative twist factors and noncanonical strengths on the OAM spectra of TPCNVPBs with *noncanonical* vortex-pair, where our attention is paid to the position of maximum weight (see the dashed box) for observing mode shifts. From Figs. 7(a3)–7(c3), the mode of maximal weight moves from $\Delta l = -2$ to 0 as μ_0 varies from 0 to -0.1 m^{-1}, which means that $\mu_0 < 0$ results in the positive movement of modes. The position of maximal weight is shifted from $\Delta l = 0$ to -3 as Q changes from $1 + 0.5\mathrm{i}$ to $1 + 5\mathrm{i}$ as shown in Figs. 7(b2) and 7(b4), which also confirms the dominance of $\Delta l < 0$ under the influence of noncanonical strength.

For clarity, we summarize the above discussion of the maximal OAM mode in Fig. 7 in Table 1.

It is worth noting that the receiving mode of $\Delta l =$ in atmospheric turbulence represents the detection probability of the signal mode of the spiral spectrum. One can clearly find that the signal mode, *i.e.*, $\Delta l = 0$, in the received plane can be jointly modulated by twist factors and noncanonical strengths to improve signal detectivity, as shown by the blue symbols in Table 1.

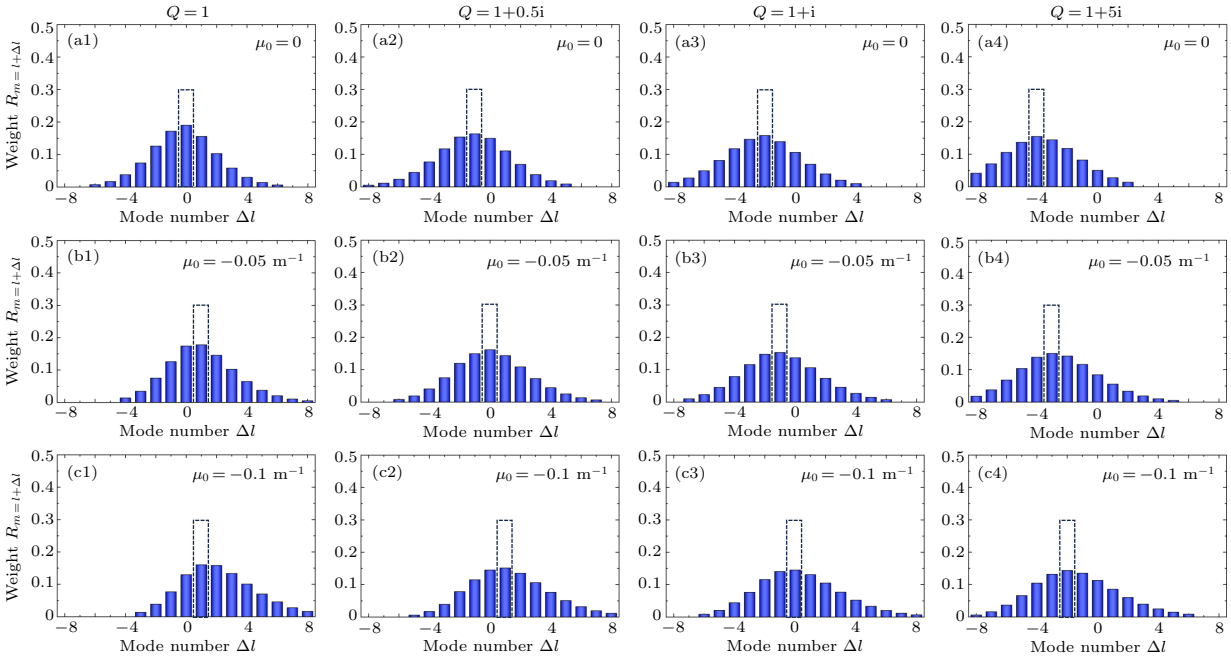


Fig. 7. The combined effect of negative twist factors and noncanonical strength on OAM spectra of TPCNVPBs with noncanonical vortex-pair at $z = 10z_0$.

Table 1. The mode at maximal weight in non-Kolmogorov atmospheric turbulence for different twist factors and noncanonical strengths at $z = 10z_0$.

	$Q = 1$	$Q = 1 + 0.5\mathrm{i}$	$Q = 1 + \mathrm{i}$	$Q = 1 + 5\mathrm{i}$
$\mu_0 = 0$	$\Delta l = 0$	$\Delta l = -1$	$\Delta l = -2$	$\Delta l = -4$
$\mu_0 = -0.05$ m^{-1}	$\Delta l = 1$	$\Delta l = 0$	$\Delta l = -1$	$\Delta l = -3$
$\mu_0 = -0.1$ m^{-1}	$\Delta l = 1$	$\Delta l = 1$	$\Delta l = 0$	$\Delta l = -2$

In addition, the twist factor in Eq. (4) is constrained by the coherence length in Eq. (5), which cannot arbitrarily twist its phase without any restriction. Figure 8 gives the OAM spectra in non-Kolmogorov atmospheric turbulence of noncanonical strength *versus* at the extreme value of twist factor $z = 10z_0$, where the extreme values are $\mu_0 = -0.044$ m^{-1} and $\mu_0 = -0.025$ m^{-1} for coherence length $\sigma = 1.5w$ and $\sigma = 2w$, respectively. The modes of maximal weight always appear at the position of $\Delta l = 0$ for the extremum of $\mu_0 = -0.044$ m^{-1} and $\mu_0 = -0.025$ m^{-1} in Figs. 8(a) and 8(b), whereas the maximal weight can continue to move from $\Delta l = -2$ to $\Delta l = -4$ by increasing the noncanonical strength Q in Figs. 8(c) and 8(d). Similar cases can also be found for the extremum of

$\mu_0 = -0.1$ m^{-1} at $\sigma = w_0$ in Figs. 7(c3) and 7(c4). When the twist factors reach their limits, the advantage in $\Delta l < 0$ caused by noncanonical strength can overcome the effects of twist factors, which also indicates that noncanonical strength plays a more significant role in signal mode modulation and detectivity compared to the twist factor.

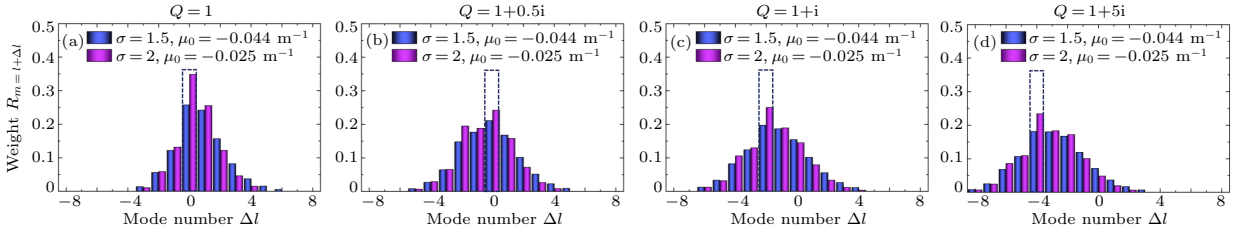


Fig. 8. OAM spectra of noncanonical strength *versus* the extreme values of twist factors for different coherent lengths at $z = 10z_0$. The extreme values are $\mu_0 = -0.044$ m^{-1} and $\mu_0 = -0.025$ m^{-1} for $\sigma = 1.5w$ and $\sigma = 2w$.

Generally, the power carried by the OAM signal mode of $\Delta l = 0$ decreases during turbulence propagation. From the detection probabilities, the crosstalk probability of other adjacent modes $\Delta l \neq 0$ increases because the power of the OAM signal mode at $\Delta l = 0$ may spread into other adjacent modes. To evaluate the combined effect of twist factor and noncanonical strength on the detection probability $R_{\Delta l}$ of the signal mode of OAM spectra in non-Kolmogorov atmospheric turbulence, the drop proportion of the signal mode is also defined as $D = 1 - R_{\Delta l}(z)/R_{\Delta l}\ (z = 0)$,[26] which can depict the power loss proportion of the signal mode at $z = 0$ propagating to the arbitrary z plane. A smaller value of D generally means better detection performance for the signal mode and shows less energy crosstalk into other modes. Tables 2 and 3 present the drop proportion of the signal mode for different twist factors and noncanonical strengths in non-Kolmogorov and Kolmogorov atmospheric turbulence propagations, respectively. For the canonical case of $Q = 1$, the drop proportions for negative twist factors are significantly lower than those for positive twist factors at a smaller propagation distance; however, the cases are reversed as the propagation distance further increases. A larger noncanonical strength can obviously decrease the drop proportions of signal modes with increasing propagation distance. For example, the value of $D = 61.53\%$ at $z = 100z_0$ under the dual influences of $\mu = -0.1$ m^{-1} and $Q = 1 + 5$i is evidently lower than $D = 78.38\%$ under $\mu = -0.1$ m^{-1} and $Q = 1$ in Table 2. Similar cases in Kolmogorov turbulence can also be found in Table 3. The results indicate that the combined effect of μ_0 and Q on the detection performance of the signal mode during long-distance turbulence propagation is distinctly better than that of only μ_0, or without μ_0 and Q.

Table 2. Drop proportions of the signal mode for different twist factors and noncanonical strengths in non-Kolmogorov atmospheric turbulence.

	$Q = 1$			$\mu = -0.1$ m^{-1}		
	$\mu_0 = 0$	$\mu_0 = -0.1$ m^{-1}	$\mu_0 = 0.1$ m^{-1}	$Q = 1+0.5$i	$Q = 1+$i	$Q = 1+5$i
$z = 20z_0$	12.46%	2.03%	14.86%	4.83%	5.97%	5.23%
$z = 40z_0$	42.38%	28.01%	34.56%	30.86%	30.62%	24.42%
$z = 60z_0$	61.28%	53.20%	46.68%	53.87%	51.60%	41.11%
$z = 80z_0$	72.18%	68.62%	55.27%	67.90%	64.81%	52.79%
$z = 100z_0$	79.04%	78.38%	62.18%	76.99%	73.40%	61.53%

Table 3. Drop proportions of the signal mode for different twist factors and noncanonical strengths in Kolmogorov turbulence.

	$Q = 1$			$\mu = -0.1$ m^{-1}		
	$\mu = 0$	$\mu = -0.1$ m^{-1}	$\mu = 0.1$ m^{-1}	$Q = 1+0.5$i	$Q = 1+$i	$Q = 1+5$i
$z = 20z_0$	4.8%	1.01%	7.0%	1.4%	2.0%	1.8%
$z = 40z_0$	26.2%	10.9%	24.9%	14.6%	15.6%	13.0%
$z = 60z_0$	47.5%	34.5%	37.7%	36.8%	36.0%	28.6%
$z = 80z_0$	61.5%	53.4%	46.8%	54.1%	51.8%	41.3%
$z = 100z_0$	70.5%	66.1%	53.9%	65.7%	62.7%	50.9%

Figure 9 provides an intuitive illustration of the competitive influence of μ_0 and Q on the detection probabilities of the signal mode in turbulence propagation. When only considering the effect of μ_0, as shown in Fig. 9(a), the extent of the reduction in detection probability $R_{\Delta l=0}$ with a larger positive μ_0, *e.g.* $\mu_0 = 0.1$ m^{-1}, is smaller than that of $\mu_0 = -0.1$ m^{-1} during long-distance propagation, and the detection probability in $\mu_0 = 0.1$ m^{-1} exceeds that in $\mu_0 = -0.1$ m^{-1} at

$z = 275$ mm. When only the dependence variable Q is present, as shown in Fig. 9(b), its power weight is only $R = 0.05$ in $Q = 1 + 5\mathrm{i}$, but its detection probability remains stable in turbulence, meaning that the embedded noncanonical strength is less sensitive to turbulence than that of the twist factor, and it can better overcome the turbulence effect on the signal mode owing to its robustness to spiral spectrum propagation. If the combined influence of μ_0 and Q is considered, as in Fig. 9(c), one can find that the power weight of $\mu_0 = -0.1$ m^{-1} and $Q = 1 + 5\mathrm{i}$ at $z = 0$ can be improved from $R = 0.05$ in Fig. 9(b) to $R = 0.11$ in Fig. 9(c), and the level of reduction of $R_{\Delta l} = 0$ is lower compared to other cases. Therefore, the combined influence of μ_0 and Q not only enhances the power weight of the signal mode at $z = 0$, but also reduces turbulence-induced degradation in the detection probabilities of the signal mode during propagation.

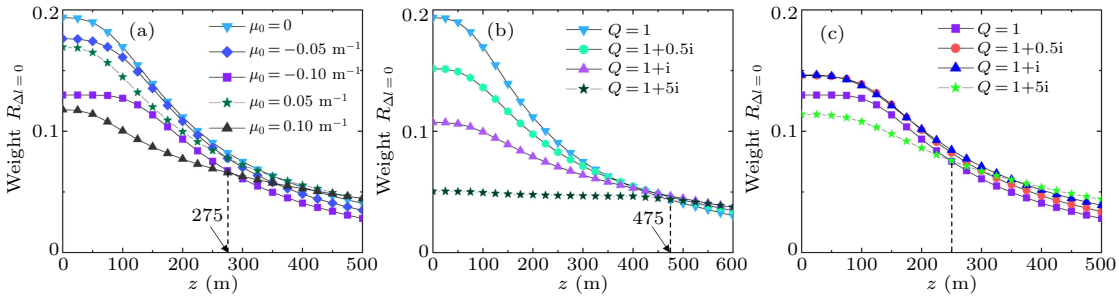


Fig. 9. Variation of detection probability of signal mode of OAM spectrum in non-Kolmogorov atmospheric turbulence for different μ_0 and Q: (a) $Q = 1$, (b) $\mu = 0$, (c) $\mu = -0.1$ m^{-1}.

4. Conclusion

By introducing a noncanonical vortex pair to the twisted partially coherent beam function, the cross-spectral densities of the resulting beams, *i.e.* (TPCNVPBs), are derived in non-Kolmogorov turbulence. The combined effects of the twist factor and noncanonical strength on spatial correlation singularities and OAM are investigated. The twist factor or noncanonical strength can lead to the creation of the so-called "distorted dislocations" in spatial correlation singularities. Noncanonical strengths can lead to an increase in the number of distorted dislocations $N \neq |l_1| + |l_2|$, but twist factors cannot affect dislocation numbers except for deepening the distortion in their structures. In turbulence propagation, the singular behaviors of topological evolution, *i.e.*, annihilation, and creation of distorted dislocations, are also found. The results may provide alternative methods to estimate turbulence intensity based on the change in the number of dislocations or the damaged structure of dislocations in turbulence propagation.

The explicit expression of the OAM flux density per photon at $z = 0$ is derived, which indicates that the noncanonical strength can further improve the OAM capacity even when the twist factor reaches its extreme value. The competitive influence of μ_0 and Q on the OAM spectra shows that noncanonical strength plays a more significant role in signal mode modulation and detectivity compared to the twist factor. If the combined effect of μ_0 and Q is considered as a whole, the detection performance of the signal mode during long-distance turbulence propagation is distinctly better than that of only μ_0, or without μ_0 and Q. In comparison with Ref. [26], where the effects of twist factors on OAM spectra were studied in anisotropic turbulence, our attention is paid to the competitive and cooperative influence of μ_0 and Q on distorted dislocation, OAM capacity, and detection probability of the signal OAM mode owing to the embedded noncanonical vortex-pair. The noncanonical strength Q exhibits more superior performance and should not be ignored. The results obtained here may provide potential applications in OAM-based optical communication, imaging, and quantum cryptography through the modulation of multiple degrees of freedom associated with noncanonical strengths and twist factors.

Appendix A

Appendix A1: Dynamic evolution of distorted dislocations of the TPCNVPBs in free space.

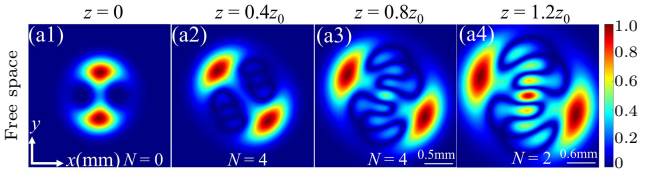


Fig. A1. Dynamics evolution of distorted dislocations of the TPCNVPBs in free space.

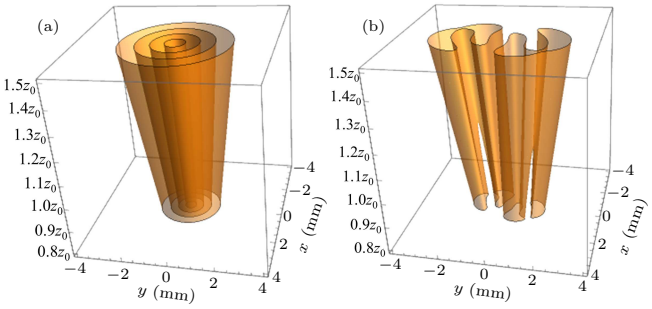


Fig. A2. The three-dimensional (3D) dynamics evolution of distorted dislocations of Figs. 3(b2)–3(b3) in turbulence propagation: (a) concentric dislocations, (b) distorted dislocations.

Appendix A2: The three-dimensional (3D) dynamical evolution of distorted dislocations from Figs. 3(b2)–3(b3) in turbulence propagation: (a) concentric dislocations, (b) distorted dislocations.

Acknowledgements

Project supported by the Natural Science Foundation of Sichuan Province, China (Grant No. 2023NSFSC0049) and the Fund from the Key Laboratories of Sensing and Application of Intelligent Optoelectronic System in Sichuan Provincial Universities (Grant No. ZNGD2401).

References

[1] Gbur G and Visser T D 2003 *Opt. Commun.* **222** 117
[2] Gbur G, Visser T D and Wolf E 2004 *J. Opt. A: Pure Appl. Opt.* **6** S239
[3] Maleev I D, Palacios D M, Marathay A S and Swartzlander G A Jr 2004 *Opt. Soc. Am. B* **21** 1895
[4] Maleev I D and Swartzlander Jr G A 2008 *J. Opt. Soc. Am. B* **25** 915
[5] Cheng K and Lv B D 2008 *J. Mod. Opt.* **55** 2751
[6] Shen Y J, Wang X J, Xie Z W, Min C J, Fu X, Liu Q, Gong M L and Yuan X C 2019 *Light: Sci. Appl.* **8** 90
[7] Dong M, Zhao C L, Cai Y J and Yang Y J 2021 *Sci. China: Phys. Mech. Astron.* **64** 224201
[8] Bai Y H, Lv H R, Fu X and Yang Y J 2022 *Chin. Opt. Lett.* **20** 012601
[9] Zhang Z, Li G Y, Liu Y L, Wang H Y, Hoenders B J, Liang C H, Cai Y J and Zeng J 2024 *Opto-Electron. Sci.* **3** 240001
[10] Palacios D M, Maleev I D, Marathay A S and Swartzlander Jr G A 2004 *Phys. Rev. Lett.* **92** 143905
[11] Yang Y J, Chen M Z, Mazilu M Mourka A, Liu Y D and Dholakia K 2013 *New J. Phys.* **15** 113053
[12] Li X F, Bashiri S, Ma Y, Liang C H, Yang Y J, Ponomarenko S A and Xu Z H 2024 *Opt. Lett.* **49** 4717
[13] Gautam A, Agarwal A K and Singh R K 2024 *Nanophotonics* **13** 4397
[14] Vanitha P, Na Y and Ko D K 2024 *J. Opt. Soc. Am. A* **41** 1397
[15] Liu Y L, Xu S Y, Peng P P, Zhang Y T, Dai S T, Chen Y H, Cai Y J and Wang F 2025 *APL Photonics* **10** 046118
[16] Allen L, Beijersbergen M W, Spreeuw R J C and Woerdman J P 1992 *Phys. Rev. A* **45** 8185
[17] Fickler R, Campbell G, Buchler B, Lam P K and Zeilinger A 2016 *Proc. Natl. Acad. Sci.* **113** 13642
[18] Padgett M J 2017 *Opt. Express* **2** 11265
[19] Gong L, Zhao Q, Zhang H, Hu X Y, Huang K, Yang J M and Li Y M 2019 *Light: Sci. Appl.* **8** 27
[20] Zhu L H, Zhang X H, Rui G H, He J, Gu B and Zhan Q W 2023 *Nanophotonics* **12** 4351
[21] Wang B Y, Han J X and Jin C 2023 *Chin. Phys. B* **32** 124208
[22] Shu L Y, Cheng K, Liao S, Liang M T and Yang C H 2023 *Chin. Phys. B* **32** 024211
[23] Peng X F, Liu L, Wang F, Popov S and Cai Y J 2018 *Opt. Express* **26** 33956
[24] Stahl C S D and Gbur G 2018 *J. Opt. Soc. Am. A* **35** 1899
[25] Zhang Y, Pan K M, Xu J, Zhu W T and Zhao D M 2021 *Opt. Commun.* **491** 126950
[26] Wang H Y, Yang Z H, Liu L, Chen Y H, Wang F and Cai Y J 2023 *Opt. Express* **31** 916
[27] Peng X F, Zhu Y G, Liu L, Wang H Y, Liu L X and Cai Y J 2025 *Opt. Express* **33** 4803
[28] Guo M X, Le W, Wang C, Rui G H, Zhu Z Q, He J and Gu B 2023 *Photonics* **10** 368
[29] Chen L L, Wang G Q, Yin Y, Zhong H Y, Liu D J and Wang Y C 2023 *Photonics* **11** 20
[30] Wang Q H, Zhang M, Zhang S H and Qu J 2025 *J. Opt. Soc. Am. A* **42** 276
[31] Liu D D, Chen L and Wang L G 2025 *Sci. Adv.* **11** eadn9279
[32] Molina-Terriza G, Wright E M and Torner L 2001 *Opt. Lett.* **26** 163
[33] Mandel L, Wolf E and Meystre P 1995 *Optical coherence and quantum optics* (Cambridge: Cambridge University Press) pp. 1438–1439
[34] Simon R and Mukunda N 1993 *J. Opt. Soc. Am. A* **10** 95
[35] Zhi D, Tao R M, Zhou P, Ma Y X, Wu W M, Wang X L and Si L 2017 *Opt. Commun.* **387** 157
[36] Wang Y K, Bai L, Xie J Y, Zhang D M, LV Q and Guo L X 2021 *Opt. Express* **29** 16056
[37] Yang Y J, Mazilu M and Dholakia K 2012 *Opt. Lett.* **37** 4949
[38] Zhang Y T, Cai Y J and Gbur G 2019 *Opt. Lett.* **44** 3617
[39] Zhang Y T, Cai Y J and Gbur G 2023 *Opt. Express* **31** 38004